Study in momentum space of phase-dependent effects on ionization of hydrogen atom interacting with short infrared laser pulses

Fréderic Ongonwou[1], Hugues Merlain Tetchou Nganso[2*], Thierry Blanchard Ekogo[1], Abdouraman[3], and Moïse Godfroy Kwato Njock[2†]

[1] *Département de Physique, Faculté des Sciences,*
Université des Sciences et Techniques de Masuku, B.P. 943 Franceville, Gabon
[2] *Atoms and Molecules Laboratory, Centre for Atomic Molecular Physics and Quantum Optics (CEPAMOQ),*
Faculty of Science, University of Douala, P.O. Box 8580, Douala, Cameroon
[3] *Institute of Condensed Matter and Nanosciences,*
Université Catholique de Louvain, 2 Chemin du Cyclotron,
Box L7.01.07, B1348 Louvain-la-Neuve, Belgium
(Dated: September 6, 2021)

We examine above-threshold ionization spectra of model atomic hydrogen in short infrared laser pulses by solving the one-electron time-dependent Schrödinger equation in momentum space. To bypass the difficulty of solving the time-dependent Schrödinger equation with the interacting nonlocal Coulomb potential, we have recently formulated an alternative *ab initio* approach [Ongonwou et al. Annals of Physics **375**, 471 (2016)], which is relied on the expansion of the atomic wavefunction and the interacting nonlocal Coulomb potential on a discrete basis set of Coulomb Sturmians in momentum space. As far as short infrared laser pulses are concerned, we have numerically evaluated the photoelectron momentum distributions, angular distributions and bound states populations. The results obtained from our accurate new computationally method are compared against predictions of other time-dependent calculations in the literature. This new theoretical model shows its sensitivity to the carrier-envelope phase of the laser pulse and captures the left-right dependence of the emitted photoelectrons momentum and angular distributions. More precisely, short pulses manifest significant dependence of the differential ionization probability on carrier-envelope phase of the laser pulse and broken forward-backward symmetry in the angular distributions.

1. INTRODUCTION

The experimental and theoretical investigations of the interaction mechanisms of atoms, molecules and clusters with intense laser fields represent one of the most challenging problems of present day research. In strong dependence on the laser parameters, very different phenomena can be observed among which the multiphoton processes, such as high-order harmonic generation (HHG) [1–3] and above-threshold ionization (ATI) (an extension of multiphoton ionization where multiple photons are absorbed to not only access the ionization continuum but to surpass the ionization potential by more than one photon) [4–8] in atomic and molecular systems. More particularly, the ionization dynamics of the atomic systems has undergone very strong development in the past decades, mainly related to the rapid progress of high powerful laser technology, namely, the possibility of generating extremely short and intense pulses. Today, with the rapid advance of modern laser technologies, lasers of various frequencies and different intensities, ultrashort and ultrafast laser pulses of duration of a few femtoseconds have opened new frontiers of science [9, 10] and are routinely available in many laboratories [11]. Studies of this highly nonlinear process of matter with strong laser pulses have revealed many interesting features of physical and chemical processes [12].

While significant progresses have been made, some issues such as the response of atoms to such laser pulses remain open. In particular, the roles of Coulomb potential, carrier-envelope phase (CEP) effects, frequency, intensity, an additional laser pulse and non-dipole effects in the dynamics of ionization are not completely clarified and certainly still hide some surprises. A challenging task was to develop a theoretical approach that takes into account the laser-matter interaction at all levels to describe these different kinds of phenomena. In this framework, it seems interesting to recall in one hand that, concerning the former, in the context of ionization dynamics, de Bohan [13, 14] and other authors [15–20] have shown the efficiency of the momentum space. As results, the wave function remains more compact and localized, the possibility to have access to ejection times of wavepackets in the continuum as well as information

———————
*htetchou@yahoo.com
†mkwato@yahoo.com

on the role of Coulomb potential on this mechanism. On other hand we mention that interest in CEP-dependent effects of few cycle laser pulses has grown since the late 1990s. Experiments on the ionization of hydrogen atom with few-cycle pulses, mainly to accurately measure CEP effects on the photoelectron spatial distributions were undertaken by Brabec and Krausz [11], Wallace et al. [21], Krausz and Ivanov [22], since the physics of these phenomena is highly relevant to attosecond science. For these experiments, the laser pulse duration was slightly shorter 5.5 fs. Experimentally, the CEP of consecutive pulses from a laser varies randomly over the entire 2π range unless some CEP stabilization technique is employed [23]. Another active stabilization technique uses the CEP dependence of strong-field photoelectron spectra to obtain the error signal [24]. One can also use optical parametric amplification to obtain high-energy pulses with passive CEP stability [25]. Achieving the goal of agreement between theory and experiment has led to validation of experimental techniques and to novel calibration methods for strong-field experiments [26]. Theoretically, calculations assume a completely characterized electric field or vector potential waveform, implying a fixed value of CEP. Telnov and Chu [27] have presented a method for calculations of electron distributions after above-threshold multiphoton ionization from the core region of a time-dependent wavepacket. They included subtle effects related to the CEP dependence of the total ionization probability and the electron energy spectra. In a recent article, Chen and co-workers [28] have used a numerical-basis-state method to solve the TDSE in strong-field physics problems. They applied the method to the hydrogen atom and reported results for excitation and ionization probabilities as well as photoelectron momentum distributions for different values of laser parameters, such as intensity, pulse length, and CEP. Suárez and collaborators [17] developed an analytical description of multiphoton processes, which extends the theoretical strong-field approximation (SFA) [29], for both the direct and rescattering transition amplitudes in atoms. As a test case, they chose a nonlocal atomic separable potential and computed both the direct and the rescattering transition amplitudes and thus the final photoelectron momentum distribution. They showed also that their model is sensitive to the CEP and can be used to efficiently extract atomic structural information and electron dynamics from measured photoelectron spectra.

In our previous paper [30], we proposed a method which proved to be fast and reliable for all practical purposes in order to understand the multiphoton processes. In this theoretical approach, we properly treated the crucial problem of the non-locality and logarithmic singularity exhibited by the Coulomb potential in the TDSE in the momentum space. Our results showed the good agreement with others results published in the literature [28, 31–37]. The aim of this paper is to use our novel spectral approach for investigating the CEP effects on photoelectron momentum and angular distributions, which properties differ significantly from those for long pulses.

The paper is organized as follows: in section 2, we give a brief description of our theoretical method, which is based on the quasianalytical solution of the 3-dimensional TDSE in the reciprocal space for the interaction of a single-active electron system exposed to an intense infrared field. This section also includes the description of ultrashort laser pulses. In section 3, we present numerical results that shed light of the asymmetry in the ionization probability density, photoelectron momentum and angular distributions resulting from ionization of the hydrogen atom by few-cycle infrared laser pulses with defined CEP. The excited state probabilities are also presented. We summarize our results and present some conclusions in section 4. Atomic units (a.u.) ($m_e = e = \hbar = 1$) are used throughout this paper unless otherwise specified.

2. THEORETICAL ATOMIC MODEL IN MOMENTUM SPACE

In this section we sketch our recently introduced methodology. In our novel model, we start from the TDSE associated with the interaction of a spin-free one-electron system exposed to an intense infrared field. Few considerations are in order here. The external electric or potential field is supposed to be linearly polarized along the unit vector $\mathbf{e}_z$, we restrict ourselves to the velocity gauge [38] and dipole approximation of the interaction between the strong laser radiation and the atomic system. Under the above considerations, the TDSE describing the dynamics of an hydrogen-like ion of nucleus charge Z exposed to such a laser field, writes in the momentum space [34]

$$\left[i\frac{\partial}{\partial t} - \frac{1}{2}\mathbf{p}^2 + (\mathbf{p} \cdot \mathbf{e}_z)A(t) \right] \Psi(\mathbf{p}, t)$$
$$- \int d\mathbf{p}' V(\mathbf{p}, \mathbf{p}') \Psi(\mathbf{p}', t) = 0, \qquad (2.1)$$

with the initial condition that the atom is in its ground state. We normalize the wavepackets in the following manner

$$\int d\mathbf{p} \mid \Psi(\mathbf{p}, t) \mid^2 = 1.$$

We use the velocity form for the laser-atom interaction Hamiltonian. The second term of the left-hand-side of equation (2.1) contains the non-local kernel $V(\mathbf{p}, \mathbf{p}')$ which is the Coulomb potential in the momentum space.

$$V(\mathbf{p}, \mathbf{p}') = -\frac{Z}{2\pi^2 \mid \mathbf{p} - \mathbf{p}' \mid^2}. \qquad (2.2)$$

The TDSE (2.1) is rendered difficult to solve by the singularity exhibited by the Coulomb potential (2.2). In order to avoid the issue of logarithmic singularity in Eq. (2.1) at $\mathbf{p} = \mathbf{p}'$, we have solved the integral equation (2.1) by means of a genuine quasi-analytical sturmian approach NCPE-SM which simplifies the resolution of this equation.

2.1. Sturmian expansion of Coulomb potential model

The detailed account of the model and all physical observables are clearly given in [30]. In what follows and in order to make our text self-contained, we only give in this section, the main step of our developments method used to determine the electron dynamics in a photoionization process. A theoretical description of this spectral method consists in expanding the atomic wavefunction and the interacting nonlocal Coulomb potential on a discrete basis set of Coulomb Sturmian functions in momentum space $\{\Phi_{n\ell m}^{\kappa}(\mathbf{p})\}$, that have interesting features very suitable for a reliable spectral approach and that we have recently constructed [30]

$$\Phi_{n\ell m}^{\kappa}(\mathbf{p}) = \Sigma_{n\ell}^{\kappa}(p)\widetilde{Y}_{\ell m}(\widehat{\mathbf{p}}), \quad \widetilde{\Phi}_{n\ell m}^{\kappa}(\mathbf{p}) = \frac{p^2 + \kappa^2}{2\kappa^2}\Phi_{n\ell m}^{\kappa}(\mathbf{p}),$$
(2.3)

$$\widetilde{Y}_{\ell m}(\widehat{\mathbf{p}}) = (-i)^{\ell} Y_{\ell m}(\widehat{\mathbf{p}}),$$
(2.4)

$$\Sigma_{n\ell}^{\kappa}(p) = \mathcal{N}_{n\ell}^{\kappa} \frac{p^{\ell}}{(p^2 + \kappa^2)^{\ell+2}} C_{\bar{n}}^{(\ell+1)}\left(\frac{p^2 - \kappa^2}{p^2 + \kappa^2}\right),$$
(2.5)

$$\mathcal{N}_{n\ell}^{\kappa} = 2^{2\ell+2}\kappa^{\ell+2}\ell! \sqrt{\frac{2\kappa n}{\pi} \frac{(n-\ell-1)!}{(n+\ell)!}},$$
(2.6)

where $C_{\bar{n}}^{(\ell+1)}$ denotes the Gegenbauer polynomial [39], $\mathcal{N}_{n\ell}^{\kappa}$ is the normalization factor, $\mathbf{p} = (p, \widehat{\mathbf{p}})$, $\widehat{\mathbf{p}} = \mathbf{p}/p$ is the unit vector directed along $\mathbf{p}$, $\widetilde{Y}_{\ell m}(\widehat{\mathbf{p}})$ is usually known as the modified spherical harmonics [40], while $\Sigma_{n\ell}^{\kappa}(p)$ denotes the radial Sturmian function in the momentum space. The quantum numbers n, ℓ, m, $\bar{n}$ and the nonlinear real parameter κ are such that $n \geq \ell + 1$, $\ell = 0, 1, 2, ..., |m| \leq \ell$, $\bar{n} = n - \ell - 1 = 0, 1, ...,$ and $0 < \kappa < 1$. These Coulomb Sturmian functions verify the following orthogonality and closure relations

$$\int_{\mathcal{P}} d\mathbf{p}\, \Phi_{n'\ell'm'}^{\kappa*}(\mathbf{p})\widetilde{\Phi}_{n\ell m}^{\kappa}(\mathbf{p}) = \delta_{n'n}\delta_{\ell'\ell}\delta_{m'm},$$
(2.7)

$$\sum_{\ell=0}^{\infty}\sum_{m=-\ell}^{\ell}\sum_{n=\ell+1}^{\infty} \Phi_{n\ell m}^{\kappa}(\mathbf{p})\widetilde{\Phi}_{n\ell m}^{\kappa*}(\mathbf{p}') = \delta(\mathbf{p} - \mathbf{p}').$$
(2.8)

We start our approach by expanding the interacting nonlocal Coulomb potential

$$V(\mathbf{p}, \mathbf{p}') = -\sum_{n\ell m} \frac{Z\kappa}{n}\widetilde{\Phi}_{n\ell m}^{\kappa}(\mathbf{p})\widetilde{\Phi}_{n\ell m}^{\kappa*}(\mathbf{p}'),$$
(2.9)

and the spectral expansion of the total wave function $\Psi(\mathbf{p}, t)$ that contains the complete information about the dynamics of the ionization process

$$\Psi(\mathbf{p}, t) = \sum_{n\ell m} c_{n\ell m}(t)\Phi_{n\ell m}^{\kappa}(\mathbf{p}),$$
(2.10)

in terms of Coulomb Sturmian functions. Inserting Eqs. (2.9) and (2.10) in Eq. (2.1) and after some manipulations, one arrives at the time-dependent matrix equation

$$i\boldsymbol{S}\frac{d}{dt}\boldsymbol{\Psi} = \boldsymbol{H}\boldsymbol{\Psi}, \quad \boldsymbol{H} = \boldsymbol{H}^{(0)} + \boldsymbol{H}^{(1)}.$$
(2.11)

where $\boldsymbol{\Psi}$ is now the vector representation of the wavefunction whose elements are the expansion coefficients $c_{n\ell m}$. $\boldsymbol{H}^{(0)}$, $\boldsymbol{S}$ and $\boldsymbol{H}^{(1)}$ are the atomic Hamiltonian, the overlap matrix and the matrix of the dipole coupling respectively and their elements are given in [30]. Since our basis functions are real, the above mentioned matrices $\boldsymbol{H}^{(0)}$, $\boldsymbol{S}$ are real symmetric and $\boldsymbol{H}^{(1)}$ is sparse while the Hamiltonian matrix $\boldsymbol{H}$ is block tridiagonal.

2.2. Description of ultrashort laser pulses

Modeling the laser pulse is a difficult choice. Several technical issues that are especially relevant for few-cycle pulses have been discussed in the literature [41], more precisely two alternative theoretical descriptions of such a pulse have retained the attention. One specifies the electric-field of the laser pulse, while the other starts from its vector potential. Therefore the pulse envelope can be associated with the vector potential $\mathbf{A}(t)$ or with the electric-field vector $\mathcal{E}(t) = (-1/c)\partial\mathbf{A}(t)/\partial t$. The zero-net-force condition $\int_{-\infty}^{\infty}\mathcal{E}(\zeta)\mathrm{d}\zeta = \mathbf{A}(-\infty) - \mathbf{A}(\infty) = -\mathbf{A}(\infty) = 0$, not only valid for this dipole approximation case, has to be satisfied.
The electric-field vector having a sine-square pulse envelope can be written following [28] (denoted LP1)

$$\mathcal{E}(t) = \mathcal{E}_0 \sin^2\left(\frac{\pi t}{T_p}\right)\sin(\omega t + \phi)\mathbf{e}_z, \mathcal{E}_0 = \sqrt{\frac{I}{I_0}},$$
(2.12)

for $0 \leq t \leq T_p$, and $\mathcal{E}(t) = \mathbf{0}$ outside this interval, where $\mathcal{E}_0$ represents the maximum field strength. We assume that the total pulse duration equals an integer number of optical cycles so that $T_p = n_c T$, where the period $T = 2\pi/\omega$, and ϕ is the CEP that specifies the delay between the maximum of the envelope and the nearest maximum of the electric field of the carrier wave with laser angular frequency ω. $I_0 = 3.5095 \times 10^{16}\ W.cm^{-2}$ denotes the atomic unit (a.u.) of laser intensity I, corresponding

to the atomic unit of electric field, $E_0 = 5 \times 10^9$ $V.cm^{-1}$ at the atomic radius $a_0 = 0.0529$ nm of the $1s$ hydrogen atom orbit. We mention here that, while $\mathcal{E}(0) = \mathcal{E}(T_p) = \mathbf{0}$, the vector potential is, in general, different from zero for $t \leq 0$ and $t \geq T_p$. However, if the total pulse duration equals an integer number n_c of laser cycles, we have $\mathbf{A}(0) = \mathbf{A}(T_p)$ so that the integral over the electric field is zero, that is, the electric field has no dc component as required. The vector potential is given by

$$\mathbf{A}(t) = [\alpha \cos(\omega t + \phi) - \alpha_+ \cos(N_+ \omega t + \phi)$$
$$-\alpha_- \cos(N_- \omega t + \phi) + (\alpha_+ + \alpha_- - \alpha) \cos \phi] \, \mathbf{e}_z, \tag{2.13}$$

$$\alpha = \frac{A_0}{2}, \quad \alpha_+ = \frac{A_0}{4N_+}, \quad \alpha_- = \frac{A_0}{4N_-}$$
$$N_\pm = \frac{n_c \pm 1}{n_c}, \quad A_0 = \frac{c\mathcal{E}_0}{\omega}. \tag{2.14}$$

A different definition of a few-cycle pulse was considered in [42]. From the point of view of integration of the TDSE it is more convenient to define a linearly polarized laser field with a sine-square envelope by its vector potential (denoted LP2)

$$\mathbf{A}(t) = A_0 \sin^2 \left(\frac{\pi t}{T_p} \right) \sin (\omega t + \phi) \, \mathbf{e}_z, \, A_0 = \frac{c}{\omega} \sqrt{\frac{I}{I_0}}, \tag{2.15}$$

for $0 \leq t \leq T_p$, and $\mathbf{A}(t) = \mathbf{0}$ outside this interval. This definition is also convenient because the zero-net-force is automatically satisfied, since the vector potential is by definition equal to zero at the beginning and at the end of the pulse, regardless of whether the number of cycles is integer or not. Therefore, this approach can be used for ultrashort pulses with non-integer n_c.

3. RESULTS AND DISCUSSION

We use the methodology outline above to study the role of the CEP on ionization of $H(1s)$ initialized from the ground state. As we choose the quantization axis along the laser polarization direction, the system has the axial symmetry during evolution, and the magnetic quantum number $m = 0$ is a constant of motion, i.e., it is conserved. Consequently, the index m introduced in Eq. (2.10) is removed from notations subsequently for further simplification,

$$\Psi(\mathbf{p}, t) = \sum_{n\ell} c_{n\ell}(t) \Sigma_{n\ell}^\kappa(p) \widetilde{Y}_{\ell 0}(\widehat{\mathbf{p}}). \tag{3.1}$$

Since the final momentum wavepacket is available, any information about the system can be easily extracted. As for NCPE-SM, a very effective and efficient numerical algorithm is employed for the high-precision solution of Eq. (2.11), namely the matrix iterative method developed by Nurhuda and Faisal [43] which is an elegant and

widely used short-time adapted Crank-Nicolson propagator [44, 45]. The wavepacket is propagated in the atomic basis, and then at the end of the laser pulse, it is rotated back to the Sturmian basis where physical observables are computed, except for the populations which are calculated in the atomic base. Concretely, for the numerical calculation, the boundaries in the sums of the orbital quantum number ℓ and the radial quantum number $\bar{n}$ take integer values varying in the intervals $(0, \ell_{max})$ and $(1, \bar{n}_{max})$, respectively. We monitored the convergence by varying the value of parameters ℓ_{max}, $\bar{n}_{max}$ and κ which limit the number of terms involved in the summations, so as to improve the calculation of the wavefunction. Full convergence in terms of the basis size has been reached in our computations with the set of optimized parameters $\bar{n}_{max} = 1500$ Sturmians per angular moment, $\ell_{max} = 31$ i.e. a total of 32 angular momenta, and the nonlinear parameter $\kappa = 0.3$. In order to study more in depth the accuracy of NCPE-SM, let us consider particularly few cases for which the dynamics are well-known. We present results of a number of runs and the results as a function of laser parameters and compare our data to those from other approaches in the literature. As before, we assume that the vector potential $\mathbf{A}(t)$ is given by the formulas (2.13) for LP1 and (2.15) for LP2. Multiphoton ionization (MPI), tunneling ionization (TI) and HHG are the basic processes that dominate laser-matter physics in this regime of intense infrared laser pulses. The above mentioned nonresonant ionization processes can be attributed to two distinct regimes based on the value of the adiabaticity parameter, the so-called Keldysh parameter [46], $\gamma = \sqrt{I_p/(2U_p)}$, with $U_p = I/(4\omega^2)$ being the ponderomotive energy, and I_p being the electron ionization potential: the perturbative regime at relatively low intensity (weak laser fields) when $\gamma \gg 1$, the multiphoton processes are the dominant mechanism, while in the strong field limit when $\gamma \ll 1$ corresponds to the tunneling regime. At the transition region when $\gamma \approx 1$ it is impossible to make a clear-cut separation between the two mechanisms. Both of them, multiphoton processes and tunnel ionization play a role. This has been confirmed experimentally and by numerical simulations. The ATI photoelectrons induced directly by the laser fields have a classical cutoff energy $2U_p$, while the electrons produced by the rescattering can extend to the maximum energy up to $10U_p$ [47, 48].

Excited-state populations

We start by applying the NCPE-SM approach to investigate the population in bound states. Figure 1 shows the n and ℓ distributions of the excited states populations resulting from the interaction of atomic hydrogen exposed to a $n_c = 2$ cycle pulse of 800 nm wavelength (photon energy, 0.057 a.u.), with a peak intensity of 1×10^{14} $W.cm^{-2}$ for different CEPs $\phi = 0$, $\pi/4$, $\pi/2$ at the end of laser pulses. The results obtained with

the LP2 are shown on the upper row, whereas, the lower row presents the LP1 results. In our present calculations, the Keldysh parameter $\gamma = 1.068$ restricts us to the transition regime. These excited-state probabilities are given as a function of the principal quantum number n (summed over $l = 0, ..., n-1$) (right panel) and the angular quantum number ℓ (left panel). The bound state populations are given in the atomic basis directly by the absolute square of the expansion coefficients for energy less than zero. Overall, at shorter pulses, it is observed that the dynamics of the excited states is both phase and shape laser field-dependent. Their distributions spread out more and more, and maxima population at different n appear, which exhibit a strong correlation of the excited-state population to the CEP of the few-cycle laser pulses. In Figs. 1(c) and (d), maxima populations are found mainly in the $(n = 4, \ell = 0)$, $(n = 5, \ell = 3)$ and $(n = 6, \ell = 5)$ excited states for CEPs $\phi = 0$, $\pi/4$, $\pi/2$ respectively, which are in agreement with the well-known conclusion for the shortest pulse, the population is distributed at the largest even-as well as odd- ℓ values, indicating that the well-known resonant character which is observed in the long pulses (that show the multiphoton character of the excitation process) of the transition is lost [49]. These results are in very good agreement with those obtained by Chen et al. [28] (see Fig. 4(a) and Fig. 5(a)). Furthermore, the $(n = 5, \ell = 3)$ is the highest point in the distribution for which excited states are populated. These findings qualitatively agree with common expectations outlined in recent works [28, 50, 51]. The preceding analysis can be extended in the case of Figs. 1(a) and (b). The results with the LP2 pulse are completely different from those obtained with the LP1 pulse. At the maximum distribution of the excited states populations, LP2 results are average about 1.9 and 2.5 orders of magnitude larger than LP1 results for P_n and P_ℓ respectively. Let us switch to analyze the $P_{n,\ell}$ distribution of the excited states produced for the same pulse as in Fig. 1. In the left panel of Fig. 2, results with LP2 are shown, whereas LP1 results are given in the right panel. It is clearly visible in this figure that the $P_{n,\ell}$ distribution of the populations is strongly correlated to the profile of the laser field. Explicitly, we note a striking difference of this distribution when passing from the laser field LP1 to the laser field LP2. We see that, as the CEP of LP1 increases from 0, $\pi/4$ to $\pi/2$, we observe a high migration of population toward a larger number of excited states with larger values of the principal quantum number, reaching values n of around 14 whereas a small number of excited states are getting populated with the laser pulse LP2.

Differential ionization probability

We investigate here the effects of CEP on ATI spectra. The investigation of these effects is timely in view of progress in laser technology. Ultrashort pulses have the advantage that the highest pulse intensity is reached in a time shorter than that which the electron needs to escape from an atom, allowing the use of much higher effective field strengths. The peak electric field of such few-cycle pulses depends on the CEP. Since the ionization process depends on the field in a highly nonlinear way, the asymmetry of the field induces an asymmetry in the emission direction of photoelectrons [52–55]. In Fig. 3 we report our investigations of ionization probability density $\mathcal{D}_{ion}(\mathbf{p}, T_p) = |\Phi_{ion}(\mathbf{p}, T_p)|^2$ obtained within the framework of NCPE-SM model. By a simple rotation of continuum-state part of the wavefunction from the atomic basis to the sturmian set, we deduce the ionized wavefunction in the sturmian basis as [30, 37]

$$\Phi_{ion}(\mathbf{p}, T_p) = \sum_{n\ell} c_{n\ell}^{ion}(T_p) \Sigma_{n\ell}^{\kappa}(p) \widetilde{Y}_{\ell 0}(\widehat{\mathbf{p}}), \qquad (3.2)$$

at the end of the pulse, for atomic hydrogen $H(1s)$ by a linearly polarized $n_c = 2$-optical cycle laser fields LP1 and LP2 with frequency $\omega = 0.057$ a.u. and peak intensity $I = 1 \times 10^{14}$ W.cm^{-2}, for various CEPs $\phi = 0$, $\phi = \pi/4$ and $\phi = \pi/2$ respectively, as a function of the canonical momentum along the polarization axis p_z for the forward ejected electrons $p_z > 0$ and backward ejected electrons $p_z < 0$. It seems worth to mention here that we have also used the conventional method for the calculation of the differential ionization probabilities which is to project the total electron wave function at the end of the laser field to the continuum states constructed by the Coulomb wave function [15, 56]. The triple differential ionization probability (photoelectron energy-angular distribution) which is the probability density for the electrons emitted with momentum $\mathbf{p} = (p, \theta, \varphi)$ into the unit energy and solid angle intervals is computed from

$$\frac{d^3\mathcal{P}}{dE d\Omega} = \sqrt{E}\mathcal{D}_{ion}(\mathbf{p}, T_p), \qquad (3.3)$$

where $d\Omega = \sin\theta d\theta d\varphi$ and $E = p^2/2$. As the system has the axial symmetry around the direction of polarization of laser field during evolution, equation (3.3) can be cast into the appropriate form

$$\frac{d^2\mathcal{P}}{dp_n dp_z} = 2\pi p_n \mathcal{D}_{ion}(\mathbf{p}, T_p). \qquad (3.4)$$

We restrict firstly the analysis to the electrons having only a canonical momentum p_z along the polarization axis, thus the transverse component p_n is set equal to zero. Under these conditions, the ponderomotive potential U_p takes the value 0.219 a.u., and the Keldysh parameter $\gamma = 1.068$. Therefore, one is in a regime where a subtle interplay between multiphoton and tunnel ionizations exists, and the dynamics of the process is not easy to discriminate. The results are displayed on a logarithmic scale in order to reveal the global ATI energy distribution. Both panels of Fig. 3 reveal the typical ATI spectra behavior. The two most prominent features highlighted in this ATI spectra are (1)-the emergence of the low ($E \leq 2U_p$) and the high or plateau

$(2U_p \leq E \leq 10U_p)$-energy patterns due to the direct and indirect ionization processes respectively [47, 53], with the expected two cutoffs defined by $2U_p$ and $10U_p$ according to the well-known three-step model [57, 58], (2)-the ability of our model to capture the CEP asymmetries, the electrons are preferentially emitted along the polarization vector and for instance, photoelectrons ejected towards the left differ substantially from those emitted to the right for the case when a few-cycle driving pulse is used. It is interesting to specify that, the spectrum of the direct and high-energy rescattered electrons do not exhibit any spatial backward-forward symmetry which is visible in Fig. 3. An obervation of the curves shows that the left-right asymmetry exists for the three values of ϕ. We have check that the left-right asymmetry becomes less and less pronounced when the number of optical cycle of field increases [37]. These results show that our NCPE-SM approach is a reliable alternative for the calculation of ATI spectra. When concentrating on the high-energy part of all these spectra, we observed the common behaviour that more high-energy electrons are emitted to the left. This result contrasts very well with what we obtained and depicted in Fig. 3 (f) where the photoelectrons ejected towards the right are clearly observed. Another interesting result is that there exists a well-defined cross-over energy where emission to the right becomes more prominent than to the left. It is worth mentioning that the CEP effects can be served as a tool for an accurate determination of the absolute phase which theoretical result should be subjected to focal averaging [59].

Electron momentum and angular distributions

In order to complete the analysis, we have extended the application of the proposed NCPE-SM theory to the study of photoelectron momentum and angular distributions for atomic hydrogen $H(1s)$ interacting with a linearly polarized 2-optical cycle laser field with frequency $\omega = 0.057$ a.u. and peak intensity $I = 1 \times 10^{14}$ W.cm^{-2} for various CEPs $\phi = 0$ (upper line), $\phi = \pi/4$ (second line), $\phi = \pi/2$ (third line) and $\phi = \pi$ (lower line). Panels on the left shows results with the pulse LP2 and Panels on the right shows results with the pulse LP1. Due to the axial or cylindrical symmetry of the atomic system, the triple differential ionization probability is independent of φ. Thus the photoelectron energy-angular distribution is described by the double differential ionization probability $d^2\mathcal{P}/dp_n dp_z$ given by Eq. (3.4) or by the angular distribution $d\mathcal{P}/d\Omega$ inferred from Eq. (3.3).
The high-resolution color contour of the double differential ionization probability and angular distributions of electrons are displayed in Figs. 4 and 5. The color density is plotted in logarithmic scale and characterizes the value of the photoelectron momentum distributions. As one can see from Figs. 4 and 5, due to the few-cycle laser field wave form, the electron trajectories strongly

depend on the CEP and the photoelectron momentum and angular distributions exhibit a clear left-right asymmetry behavior with respect to the $p_z = 0$ momentum which can be understood with the occurrence and interference of only a few emission and rescattering events [17]. Fig. 4 shows that the photoelectron momentum distribution is no ring shaped and is squeezed along the laser field direction. Strictly speaking, one could say that the photoelectron momentum distribution is in deformed arc structure shaped. Thus indicates that the photoelectron momentum distribution strongly depends on the direction for the specified laser-pulse parameters. Moreover, when the absolute phase of the fields takes the values $\phi = 0$ and $\phi = \pi/4$, the backward emission of electrons is preponderant while the forward emission emerges when $\phi = \pi$. In the particular case of $\phi = \pi/2$, the ejection of the electron into the continuum is laser field shape dependent. The electrons are mostly emitted to the left for LP2 laser field shape and to the right for LP1's one.

4. SUMMARY AND OUTLOOK

It has been shown that the momentum space is, despite the non-locality of the atomic potential, actually well suited to probe the ionization dynamics and the atomic potential effects. It highlights, in fact, a quasi-instantaneous viewing of the process since at the first sight, ionization happens first in terms of moment before being in terms of position. In other word, working in the momentum space, provides direct information on the ionization dynamics and in particular on the time at which the electron is emitted. We have developed an efficient *ab initio* NCPE-SM method of solving the TDSE directly in the momentum space. It should be pointed out that to date this is the only approach which analytically eliminates the singularities of the kernel of the integrodifferential equation. We have adopted the velocity form of the laser-atom interaction and our theory goes far beyond the well-known SFA. A theoretical description of the NCPE-SM spectral method consists in expanding the atomic wavefunction and the interacting nonlocal Coulomb potential on a discrete basis set of Coulomb Sturmian functions in momentum space. Our novel model provides on one hand simple frameworks for MPI and ATI understanding, which are in agreement with the available experimental observations and the previous theoretical approaches, and on the other hand, has drawbacks and advantages [30, 34, 35, 37]. Due to the highly efficient numerical algorithm for the computation of the total wavepackets, we have been able to gain insights in the photoelectron momentum and angular distributions of ATI as well as excitation probabilities in a regime of intense ultrashort low-frequency laser pulse. From these investigations, it emerges the following two clear observations - photoelectron spectra show the two well-known cutoffs which are ubiquitously present in atomic ATI [47, 53] - our novel model captures

the left-right dependence or asymmetry of the emitted photoelectrons momentum and angular distributions. It thus shows its sensitivity to the CEP of the laser pulse. The ability to capture this dependence and its features is especially important for applications to methods such as Laser-induced electron diffraction (LIED), which relies on large momentum transfers and backscattered electron distributions. As another interesting perspectives, (1) the NCPE-SM spectral treatment will be extended to basis set of B-spline functions. This new representation could be useful to explore multiphoton processes in hydrogen atom, (2) the NCPE-SM model will also be extended to include other aspects such as nondipole corrections. These questions, surely not easy tasks will be addressed in the forthcoming publications.

[1] Gaarde, M. B.; Antoine, Ph.; LHuillier, A.; Schafer, K. J.; Kulander, K. C. Phys. Rev. A 1998, 57, 4553.

[2] Tate, J.; Auguste, T.; Muller, H. G.; Salires, P.; Agostini, P.; DiMauro, L. F. Phys. Rev. Lett. 2007, 98, 013901.

[3] Ciappina, M. F.; Biegert, J.; Quidant, R.; Lewenstein, M. Phys. Rev. A 2012, 85, 033828.

[4] Kulander, K. C. Phys. Rev. A 1987, 35, 445.

[5] Muller, H. G. Phys. Rev. A 1999, 60, 1341.

[6] Bauer, D. Phys. Rev. Lett. 2005, 94, 113001.

[7] Blaga, C. I.; Catoire, F.; Colosimo, P.; Paulus, G. G.; Muller, H. G.; Agostini, P.; DiMauro, L. F. Nature Phys. 2009, 5, 335.

[8] Ruf, M.; Bauke, H.; Keitel, C. H. J. Comput. Phys. 2009, 228, 9092.

[9] Agostini, P.; DiMauro, L. F. Rep. Prog. Phys. 2004, 67, 813.

[10] Scrinzi, A.; Ivanov, M. Yu.; Kienberger, R.; Villeneuve, D. M. J. Phys. B 2006, 39, R1.

[11] Brabec, T.; Krausz, F. Rev. Mod. Phys. 2000, 72, 545.

[12] Protopapas, M.; Keitel, C. H.; Knight, P. L. Rep. Prog. Phys. 1997, 60, 389.

[13] de Bohan, A. PhD Thesis, Université Catholique de Louvain, Belgium, 2001.

[14] de Bohan, A.; Piraux, B.; Ponce, L.; Taïeb, R.; Véniard, V.; Maquet, A. Phys. Rev. Lett. 2002, 89, 113002.

[15] Zhou, Z.; Chu, S. -I. Phys. Rev. A 2011, 83, 013405.

[16] Becker, W.; Long, S.; McIver, J. K. Phys. Rev. A 1994, 50, 1540.

[17] Suárez, N.; Chacón, A.; Ciappina, M. F.; Biegert, J.; Lewenstein, M. Phys. Rev. A 2015, 92, 063421.

[18] Suárez, N.; Chacón, A.; Ciappina, M. F.; Wolter, B.; Biegert, J.; Lewenstein, M. Phys. Rev. A 2016, 94, 043423.

[19] Suárez, N.; Chacón, A.; Pérez-Hernández, J. A.; Biegert, J.; Lewenstein, M.; Ciappina, M. F. Phys. Rev. A 2017, 95, 033415.

[20] Suárez, N.; Chacón, A.; Pisanty, E.; Ortmann, L.; Landsman, A. S.; Picón, A.; Biegert, J.; Lewenstein, M.; Ciappina, M. F. Phys. Rev. A 2018, 97, 033415.

[21] Wallace, W. C. et al. New J. Phys. 2013, 15, 033002.

[22] Krausz, F.; Ivanov, M. Rev. Mod. Phys. 2009, 81, 163.

[23] Baltuška, A.; Uiberacker, M.; Goulielmakis, E.; Kienberger, R.; Yakovlev, V. S.; Udem, T.; Nansch, T. W. H.; Krausz, F. IEEE J. Sel. Top. Quant. Elec. 2003, 9, 972.

[24] Adolph, D.; Sayler, A. M.; Rathje, T.; Nuhle, K. R.; Paulus, G. G. Opt. Lett. 2011, 36, 3639.

[25] Vozzi, C. et al. Opt. Express 2006, 14, 10109.

[26] Kielpinski, D.; Sang, R. T.; Litvinyuk, I. V. J. Phys. B: At. Mol. Opt. Phys. 2014, 47, 204003.

[27] Telnov, D. A.; Chu, S. -I. Phys. Rev. A 2009, 79, 043421.

[28] Chen, S.; Gao, X.; Li, J.; Becker, A.; Jaroń-Becker, A. Phys. Rev. A 2012, 86, 013410.

[29] Ammosov, M. V.; Delone, N. B.; Krainov, V. P. Sov. Phys. JETP, 1986, 64, 1191.

[30] Ongonwou, F.; Tetchou Nganso, H. M.; Ekogo, T. B.; Kwato Njock, M. G. Annals of Physics 2016, 375, 471.

[31] Hamido, A.; Eiglsperger, J.; Madroñero, J.; Mota-Furtado, F.; O'Mahony, P. F.; Frapiccini, A. L.; Piraux, B. Phys. Rev. A 2011, 84, 013422.

[32] Hamido, A. Ph.D. Thesis, Université catholique de Louvain, Belgium, 2014. available at http://hdl.handle.net/2078.1/153485.

[33] Tetchou Nganso, H. M. Ph.D. Thesis, Université Catholique de Louvain, Belgium, 2010.

[34] Tetchou Nganso, H. M.; Popov, Yu. V.; Piraux, B.; Madroñero, J.; Kwato Njock, M. G. Phys. Rev. A 2011, 83, 013401.

[35] Tetchou Nganso, H. M.; Hamido, A.; Kwato Njock, M. G.; Popov, Yu. V.; Piraux, B. Phys. Rev. A 2013, 87, 013420.

[36] Tetchou Nganso, H. M.; Giraud, S.; Piraux, B.; Popov, Yu. V.; Kwato Njock, M. G. J. Elect. Spect. Rel. Phen. 2007, 161, 178.

[37] Ongonwou, F.; Ekogo, T. B.; Tetchou Nganso, H. M.; Abdouraman.; Wafo Soh, C.; Kwato Njock, M. G. Annals of Physics 2021 (submitted).

[38] Cormier, E.; Lambropoulos, P. J. J. Phys. B 1996, 29, 1667.

[39] Gradshteyn, I. S.; Ryzhik, I. M. Table of Integrals, Series and Products, Academic Press, New York, 1965.

[40] Varshalovich, D. A.; Moskalev, A. N.; Khersonskii, V. K. Quantum Theory of Angular Momentum, World Scientific, Singapore, 1988.

[41] Miloševií, D. B. ; Paulus, G. G.; Becker, W. Laser Phys. 2003, 13, 948.

[42] Telnov, D. A.; Chu, S. -I. Phys. Rev. A 2019, 100, 043423.

[43] Nurhuda, M.; Faisal, F. H. M. Phys. Rev. A 1999, 60, 3125.

[44] Goldberg, A.; Schey, H. M.; Scwartz, J. L. Amer. J. Phys. 1967, 35, 177.

[45] Koonin, S. E.; Meredith, D. C. Computational Physics: Fortran Version, Addison-Wesley, Redwood City, CA, 1990.

[46] Keldysh, L. V. Zh. Eksp. Teor. Fiz. 1964, 47, 1945 [Sov. Phys. JETP 1965, 20, 1307].

[47] Lewenstein, M.; Kulander, K. C.; Schafer, K. J.; Bucksbaum, P. H. Phys. Rev. A 1995, 51, 1495.

[48] Kamiński, J. Z.; Jaroń, A.; Ehlotzky, F. Phys. Rev. A 1996, 53, 1756.

[49] Piraux, B.; Mota-Furtado, F.; O'Mahony, P. F.; Galstyan, A.; Popov, Yu. V. Phys. Rev. A 2017, 96, 043403.

[50] Nakajima, T.; Watanabe, S. Phys. Rev. Lett. 2006, 96, 213001.

[51] Nakajima, T.; Watanabe, S. Opt. Lett. 2006, 31, 1920.

[52] Paulus, G. G.; Grasbon, F.; Walther, H.; Villoresi, P.; Nisoli, M.; Stagira, S.; Priori, E.; Silvestri, S. D. Nature (London) 2001, 414, 182.

[53] Miloševií, D. B. ; Paulus, G. G.; Bauer, D.; Becker, W. J. Phys. B: At. Mol. Opt. Phys. 2006, 39, R203.

[54] Miloševií, D. B. ; Paulus, G. G.; Becker, W. Phys. Rev. Lett. 2002, 89, 153001.

[55] Martiny, C. P. J.; Madsen, L. B. Phys. Rev. Lett. 2006, 97, 093001.

[56] Cormier, E.; Lambropoulos, P. J. J. Phys. B 1997, 30, 77.

[57] Schafer, K. J.; Yang, B.; DiMauro, L. F.; Kulander, K. C. Phys. Rev. Lett. 1993, 70, 1599.

[58] Corkum, P. B. Phys. Rev. Lett. 1993, 71, 1994.

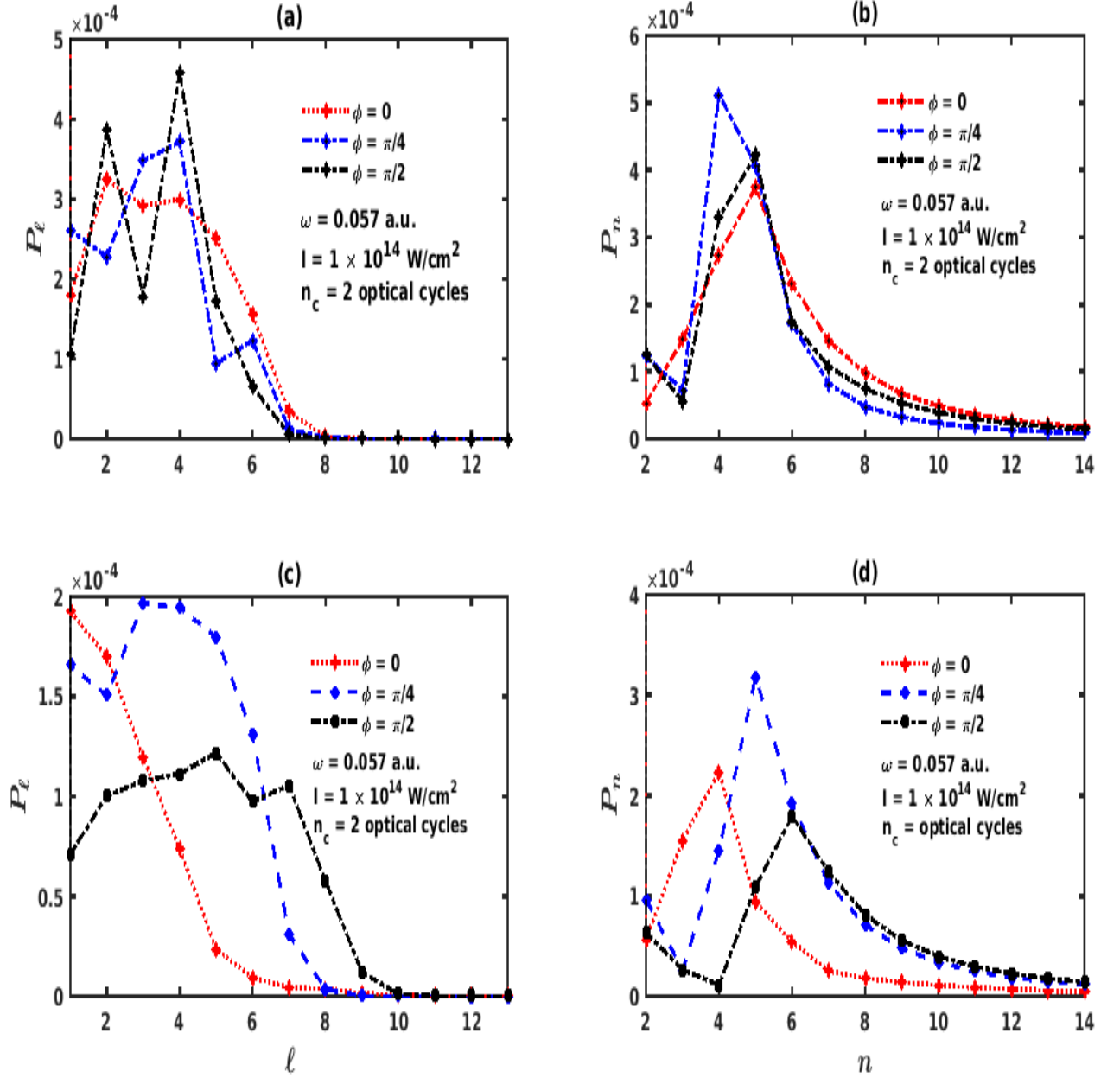[59] Chelkowski, S.; Bandrauk, A. D. Phys. Rev. A 2005, 71, 053815.

FIG. 1: (Color online) Excited-state populations at the end of the pulse, resulting from the atomic hydrogen $H(1s)$ driven by a linearly polarized 2-optical cycle laser field with frequency $\omega = 0.057$ a.u. and peak intensity $I = 1 \times 10^{14}$ W.cm^{-2} for various CEPs $\phi = 0$ (red dotted line with full circles), $\phi = \pi/4$ (blue dashed line with full circles (upper row) and with hatched diamonds (lower row)), $\phi = \pi/2$ (black dashed-dotted line with full circles (upper row) and with solid squares (lower row)). They are given as a function of the angular momentum quantum number ℓ (Panels on the left (a) and (c)) and as a function of the principal quantum number n (Panels on the right (b) and (d)). The first row shows NCPE-SM results with the pulse LP2 and the second row shows NCPE-SM results with the pulse LP1. The symbol is connected with lines to guide the eye.
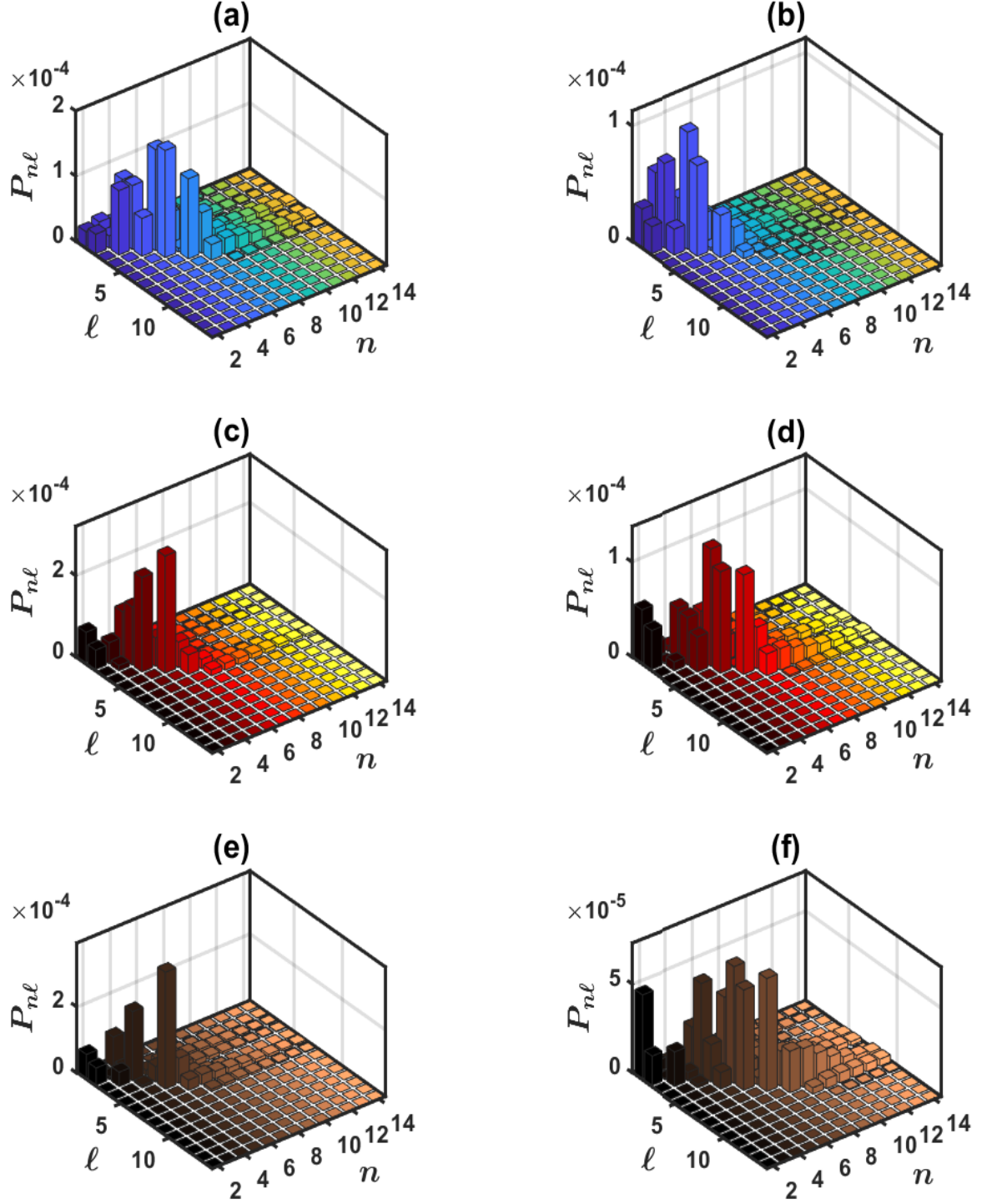
FIG. 2: (Color online) Distribution of the populations as a function of the angular momentum quantum number ℓ and the principal quantum number n at the end of the pulse, for atomic hydrogen $H(1s)$ interacting with a linearly polarized 2-optical cycle laser field with wavelength of 800 nm. The peak intensity is fixed at $I = 1 \times 10^{14}$ W.cm^{-2} and a CEP $\phi = 0$ (upper line (a) and (b)), $\phi = \pi/4$ (middle line (c) and (d)), and $\phi = \pi/2$ (lower line (e) and (f)). Left column shows NCPE-SM results with the pulse LP2 and right column shows NCPE-SM results with the pulse LP1.
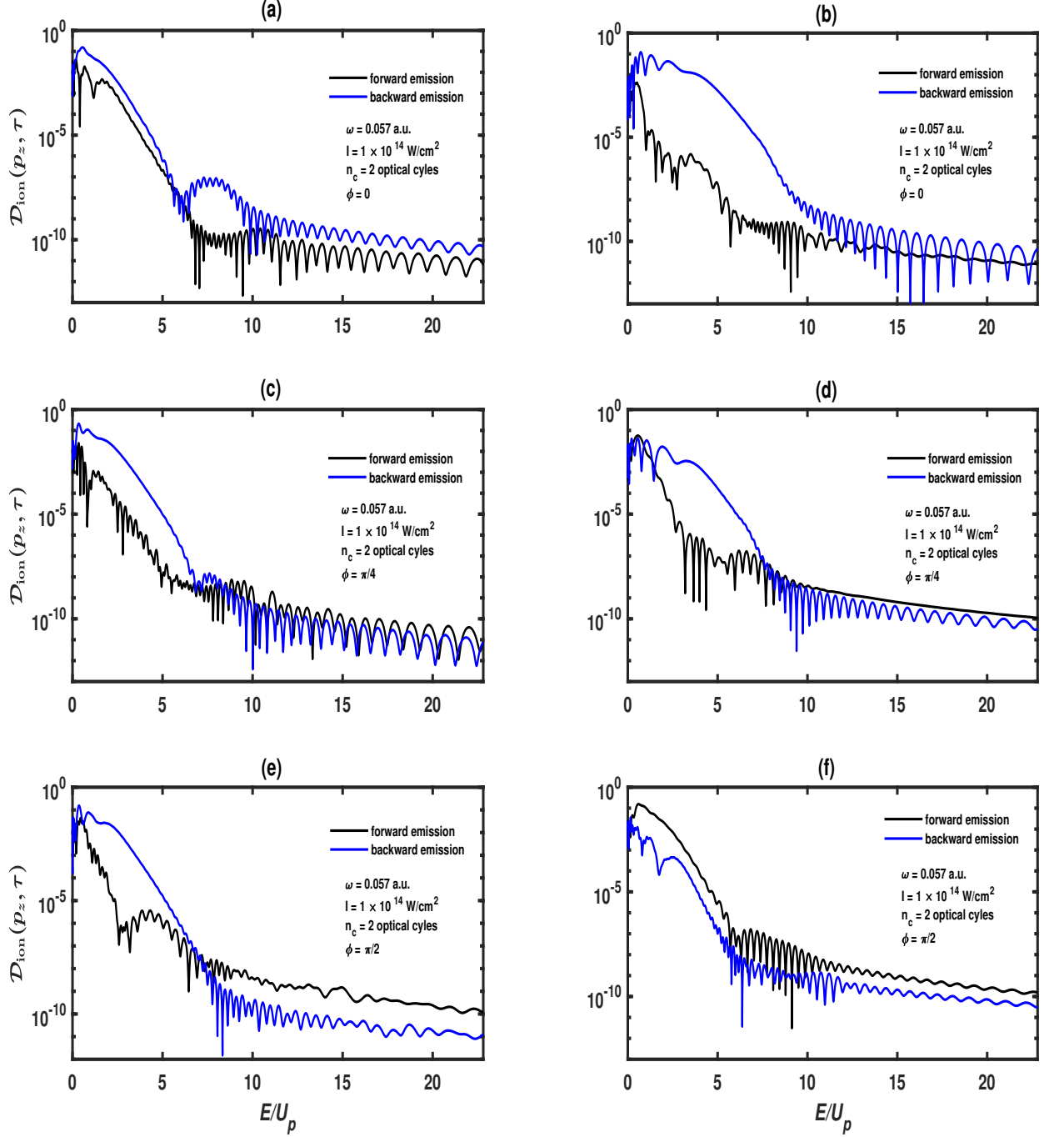
FIG. 3: (Color online) Left (blue solid line) and right (black solid line) ionization probability density (in logarithm scale) at the end of the pulse, for atomic hydrogen $H(1s)$ by a linearly polarized 2-optical cycle laser field with frequency $\omega = 0.057$ a.u. and peak intensity $I = 1 \times 10^{14}$ W.cm^{-2} for various CEPs $\phi = 0$ (upper line (a) and (b)), $\phi = \pi/4$ (second line (c) and (d)), and $\phi = \pi/2$ (lower line (e) and (f)). Panels on the left shows NCPE-SM results with the pulse LP2 and Panels on the right shows NCPE-SM results with the pulse LP1.
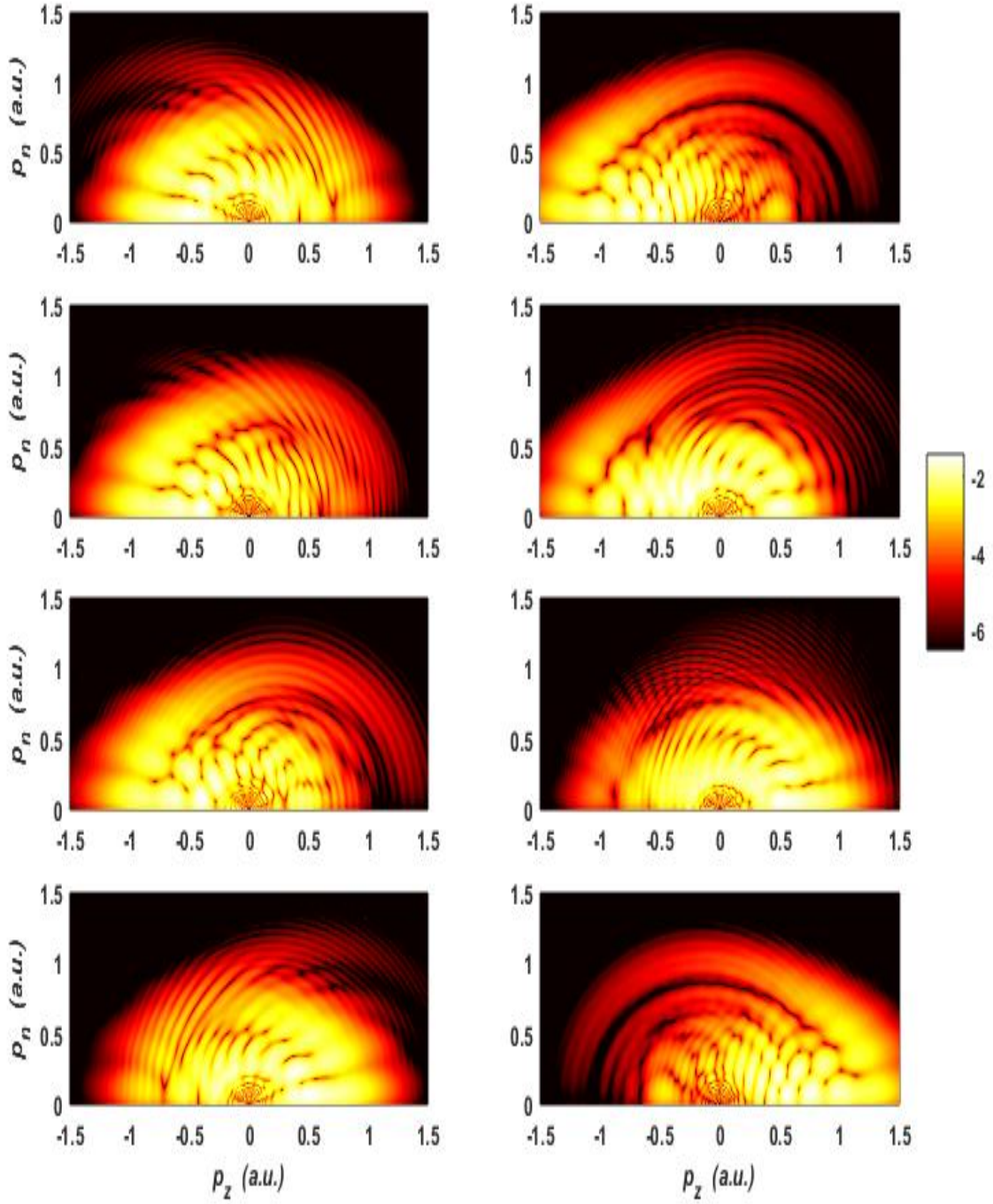
FIG. 4: (Color online) Double differential electron momentum distributions (in logarithmic scale) in cylindrical coordinates (p_z, p_n) at the end of the pulse, in photodetachment from hydrogen atom $H(1s)$ by a linearly polarized 2-optical cycle laser field with frequency $\omega = 0.057$ a.u. and peak intensity $I = 1 \times 10^{14}$ W.cm^{-2} for various CEPs $\phi = 0$ (upper line), $\phi = \pi/4$ (second line), $\phi = \pi/2$ (third line) and $\phi = \pi$ (lower line). Panels on the left shows NCPE-SM results with the pulse LP2 and Panels on the right shows NCPE-SM results with the pulse LP1.
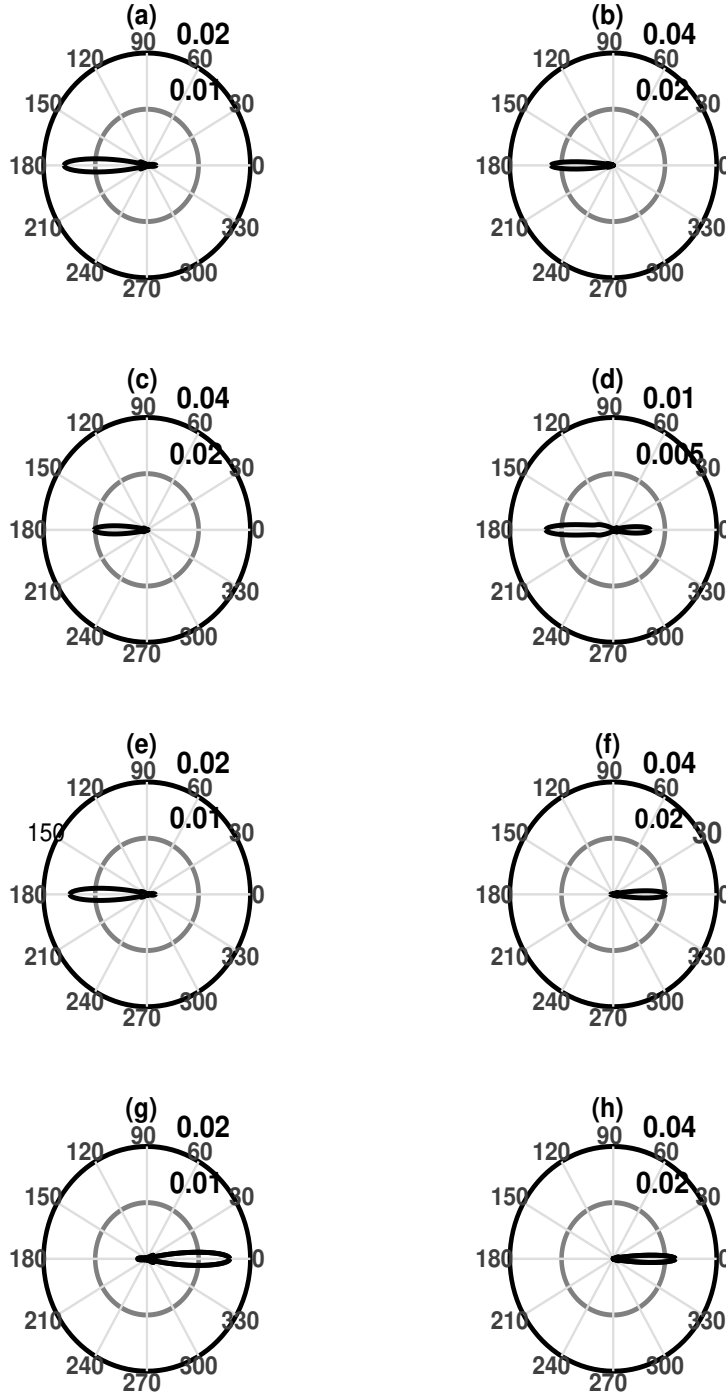
FIG. 5: Photoelectron angular distributions at the end of the
pulse, for atomic hydrogen $H(1s)$ interacting with a linearly
polarized 2-optical cycle laser field with wavelength of 800 nm
and peak intensity $I = 1 \times 10^{14}$ W.cm^{-2} for various CEPs
$\phi = 0$ (upper line), $\phi = \pi/4$ (second line), $\phi = \pi/2$ (third
line) and $\phi = \pi$ (lower line). Panels on the left shows NCPE-
SM results with the pulse LP2 and Panels on the right shows
NCPE-SM results with the pulse LP1.